Exciton fine structure in CdSe nanoclusters

K. Leung,* S. Pokrant,† and K. B. Whaley
Department of Chemistry, University of California at Berkeley, Berkeley, California 94720
(Received 29 October 1997; revised manuscript received 31 December 1997)

The fine structure in the CdSe nanocrystal absorption spectrum is computed by incorporating two-particle electron-hole interactions and spin-orbit coupling into a tight-binding model, with an expansion in electron-hole single-particle states. The exchange interaction and spin-orbit coupling give rise to dark, low-lying states that are predominantly triplet in character, as well as to a manifold of exciton states that are sensitive to the nanocrystal shape. Near the band gap, the exciton degeneracies are in qualitative agreement with the effective mass approximation (EMA). However, instead of the infinite lifetimes for dark states characteristic of the EMA, we obtain finite radiative lifetimes for the dark states. In particular, for the lowest, predominantly triplet, states we obtain radiative lifetimes of microseconds, in qualitative agreement with the experimental measured lifetimes. The resonant Stokes shifts obtained from the splitting between the lowest dark and bright states are also in good agreement with experimental values for larger crystallites. Higher-lying states exhibit significantly more complex behavior than predicted by EMA, due to extensive mixing of electron-hole pair states. [S0163-1829(98)06619-3]

I. INTRODUCTION

The exciton fine structure in CdSe nanocrystals has received extensive attention.[1–8] The electron-hole exchange interaction is strongly enhanced in nanocrystals by the quantum confinement, and can reach tens of meV. This gives rise to dark, triplet states below the absorbing singlet manifolds. The existence of interior dark states is consistent with the observation of a Stokes shift in luminescence experiments,[1,3] which was originally attributed to surface trapping states.[9] These nominally ''dark'' states have small but finite oscillator strengths, as a result of symmetry breaking mechanisms that mix singlets and triplets, such as spin-orbit and exciton-phonon couplings.

The crystallite shape asymmetry and crystal-field splitting of the wurtzite lattice further complicates this picture. The roles played by the various contributions have recently been analyzed using the effective mass approximation (EMA).[1,4] In direct gap materials such as CdSe, the exciton is assumed to be made up of valence (hole) p states and conduction (electron) s states. The spin-orbit spitting is large, and to a first approximation, the lowest-lying exciton with hole angular momentum $j=3/2$ is eightfold degenerate in spherical crystallites.[4] Lattice field effects, deviation from spherical crystallite symmetry, and the exchange interaction split these into five levels, two of which are dark.[1,3] EMA calculations based on a perturbative splitting of the degeneracy of the first electron-hole state by these factors have successfully accounted for fine structures observed in photoluminescence excitation and fluorescence line narrowing experiments, and give quantitative agreement with the resonant Stokes shifts for larger crystallites.[1,10] However, the EMA predicts infinite lifetimes for the dark states, in contradistinction to the experimentally observed microsecond lifetimes,[1] and appears to give too small values for the resonant shifts at small cluster sizes. Furthermore, the magnitude of the nonresonant Stokes shifts seen upon absorption above the band edge is also not accounted for by EMA. Other factors such as coupling to phonons therefore have to be invoked within an EMA analysis to account for these features.[1,10]

In general, the neglect of the atomic nature of the nanocrystals within EMA places restrictions on the level of detail that can be derived from such analysis. This becomes increasingly important as the crystal size decreases, since both the validity of an envelope function approximation and the neglect of surface effects then become questionable. Several nonessential but serious, additional approximations are commonly implemented within EMA in order to retain its simplicity. In the EMA fine-structure calculations of Ref. 1 the mixing of electron-hole pair states away from the band edge into the lowest exciton states is neglected, the Coulomb interaction is neglected, and the electron-hole exchange interaction is approximated by a zero range function. Recent dipole moment measurements of CdSe nanocrystal colloids[11] and observation of parity-forbidden two-photon transitions[27] imply non-negligible mixing of the band-edge hole state with states deeper in the valence band, which suggests that a reexamination of the effect of higher electron-hole pair states on the band-edge exciton would be useful. Incorporation of these higher states has consequences for the treatment of the Coulomb interaction. While for singlet and triplet levels derived from a single electron-hole pair state the Coulomb terms contribute equally and appear to cancel, omission of the Coulomb terms becomes serious when coupling between electron-hole pair states is allowed, since it reassigns the oscillator strengths and reorders the single-particle states.

In this paper, we therefore compute the two-particle absorption spectra of a series of CdSe nanocrystals using tight-binding models within a configuration interaction representation. This allows us to go beyond the EMA, albeit in a semiempirical framework, and to examine the validity of the EMA assumptions. In particular, we demonstrate here effects of coupling between the lowest electron-hole pair states to higher-lying states on the low-lying excitonic manifold, as well as the effect of the atomic nature of the band-edge wave functions on the lowest exciton states. A key consequence of the latter is the mixing in of singlet character into the nominally ''dark'' triplet, resulting in finite radiative lifetimes that

agree quantitatively with the microsecond experimental estimates[1] without introducing nonradiative effects.

Previous tight-binding calculations on CdSe have considered spherical or tetrahedral crystallites in the zinc-blende structure.[12–16] Some of these studies incorporated the effect of the electron-hole Coulomb interaction on excitonic states, either perturbatively,[15] or nonperturbatively,[13,14] but a full analysis of the excitonic fine structure deriving from incorporation of spin degrees of freedom has not yet been made for CdSe within tight binding. In this work we use the restricted basis set diagonalization method[17,18] to compute the effects of Coulomb, exchange, and spin-orbit coupling. In accordance with the results of recent high-resolution transmission electron microscopy (TEM) experiments,[19] we model the crystallites here as slightly prolate tops with wurtzite lattice architecture. The crystallite shape and the C_{3v} lattice symmetry are therefore already incorporated at the single-particle level, unlike in EMA where they are added as perturbative terms.[1] Our aim in the present paper is to first isolate the relative effects of discrete lattice structure, shape, and spin-orbit and exchange couplings on the exciton fine structure, with several series of size-dependent studies for various aspect ratios. Since we are not explicitly concerned with surface effects here, we simplify the surface description and in the calculations described in this paper truncate the surface by removing the dangling orbitals. It is expected, and there is some experimental evidence for this, that the presence of dangling orbitals leads to surface relaxation in CdSe nanocrystals.[20] We have also studied the effect of such relaxation on the fine structure by carrying out total-energy minimization of our tight-binding nanocrystals. The consequences of this for the excitonic fine structure will be discussed briefly below, but a detailed analysis of the molecular structure of the surface and its reconstructions is postponed to a later publication.[21]

This paper is organized as follows. Section II describes the model CdSe crystallites we use and the method of calculation. Section III contains the results, and Sec. IV concludes the paper with further discussions.

II. THEORY AND MODEL

A. Tight-binding model of CdSe nanocrystals

We focus on four series of CdSe nanocrystals, A–D, all governed by the same semiempirical tight-binding model described below. Their sizes range from 238–1236 atoms (radii $\sim$9–18 Å). The crystallites have C_{3v} symmetry and are all prolate in shape (see Fig. 1). The z axis is regarded as the long (C_{3v}) axis. Series A, B, and C have moments of inertia determined by a constant ratio, given by the values (1.05 $\pm$0.01:1:1), (1.2$\pm$0.02:1:1), and (1.44$\pm$0.06:1:1) respectively. Thus the asphericity increases from A to C, with series A being near spherical and series C being most prolate. The last series (D) has moments of inertia ratios corresponding (within $\pm$0.03) to the analytically fit distribution of Ref. 1. In that fit, it was assumed that the crystallites are ellipsoids with one long axis of length c and two short axes of length b, giving an ellipticity $\mu = c/b - 1$, which was seen to increase with nanocrystal size, i.e., smaller crystals were more spherical and the larger crystals more prolate. Reference 1 gives

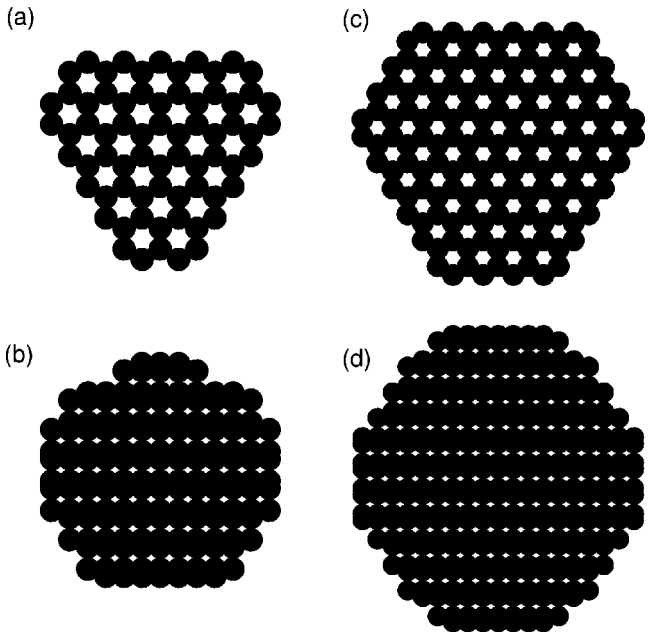

FIG. 1. Ball-and-stick models of CdSe clusters from series D. (a) 387 atoms, ellipticity $\mu_{\rm mir}=1.03$, top view (along the C_{3v} axis); (b) 387 atoms, side view; (c) 1194 atoms, ellipticity $\mu_{\rm mir}=1.09$, top view; (d) 1194 atoms, side view.

$$\mu(a) = 0.101 - 0.034a + 3.507\times10^{-3}a^2 - 1.177\times10^{-4}a^3 + 1.863\times10^{-6}a^4 - 1.418\times10^{-8}a^5 + 4.196\times10^{-11}a^6, \quad (1)$$

where $a=(b^2c)^{1/3}/2$ is the effective radius.

For series D in this work we first estimate the moments of inertia assuming an ellipsoidal structure with axes c, b, and b. A moments of inertia ratio $(c/b)^2$:1:1 corresponds then to a length-to-width ratio c/b and hence to ellipticity $\mu_{\rm mir}=c/b-1$. Thus series A, B, and C are characterized by ellipticity $\mu_{\rm mir}=0.025$, 0.095, and 0.20, respectively. For series D the value of $\mu_{\rm mir}$ is matched to the prediction of Eq. (1) for given crystallite sizes (see Table I). We see here that series D is near spherical for small sizes, and becomes prolate to the same extent as series B for the largest sizes.

For comparison, in Table I we also list the true length-to-width ratios, which we refer to as $(\mu_{\rm physical}+1)$. We do not consider these length-to-width ratios directly in this work because such a procedure can produce misleading shape assignments for the size range considered here. This is a consequence of the fact that our model contains discrete atoms, so that the length-to-width ratio cannot be continuously tuned to Eq. (1). For example, adding a bilayer of Cd-Se atoms in the z direction increases the long axis by 3.5 Å. For the largest crystallite studied here, which is 37 Å in diameter, this represents a 10% change in the length-to-width ratio, i.e., a change of 0.1 in $(\mu_{\rm physical}+1)$. However, the moments-of-inertia ratio is much less sensitive to such shape variations. For example, the 244- and 246-atom clusters have true length-to-width ratios differing by 20% (column 5 in

TABLE I. Aspect ratios of series D crystallites, $c/b=\mu+1$, as measured from the square root of the moments-of-inertia ratio ($\mu_{\rm mir}+1$) and from the length-to-width ratio ($\mu_{\rm physical}+1$). $\mu_{\rm expt}=\mu(a)$ is the experimental ellipticity estimate from the polynomial fit in Eq. (1) (Ref. 1). The effective radius a is defined by $a=(b^2c)^{1/3}/2$.

No. atoms	a (Å)	$\mu_{\rm expt}+1$	$\mu_{\rm mir}+1$	$\mu_{\rm physical}+1$
238	10.4	1.01	1.00	1.10
244	10.4	1.01	1.01	1.10
246	9.8	1.01	1.02	0.93
325	12.2	1.03	1.02	0.93
351	12.2	1.03	1.03	0.93
377	12.2	1.03	1.04	0.93
387	12.2	1.03	1.03	1.08
389	12.2	1.03	1.04	1.08
398	12.2	1.03	1.04	1.08
414	12.7	1.03	1.02	1.11
510	14.0	1.04	1.03	1.06
549	14.0	1.05	1.04	1.06
552	14.0	1.05	1.02	1.06
558	14.0	1.05	1.04	1.06
570	14.0	1.05	1.04	1.06
594	14.0	1.05	1.04	1.06
600	14.0	1.05	1.03	1.06
636	14.0	1.05	1.03	1.06
823	15.9	1.08	1.06	1.04
868	15.9	1.08	1.06	1.04
871	15.9	1.08	1.07	1.04
1178	17.8	1.09	1.09	1.04
1194	18.3	1.11	1.09	1.14
1236	18.3	1.11	1.12	1.14

Table I), but the ellipticities derived from the moments-of-inertia ratios differ only by 1% (1.01 and 1.02, respectively, column 4 in Table I). The difference in length-to-width ratio stems from a small ''cap'' at the top face of the 246-atom cluster that increases its long axis by 3.5 Å relative to that of the 244-atom cluster. This small number of atoms has, however, a smaller percentage effect on the moments-of-inertia ratios and hence also on $\mu_{\rm mir}$, the ellipticity derived from this. It will be shown below that, despite the significant difference in aspect ratios, the physical properties of these two clusters are very similar and therefore the moments-of-inertia-derived ellipticity $\mu_{\rm mir}$ appears to be a better indicator of their electronic shape. The values of $\mu_{\rm physical}+1$ in Table I thus systematically show larger deviations from $\mu_{\rm expt}$.

The orbital basis used in the tight-binding model is $\{s,p_x,p_y,p_z,s^*\}$. The tight-binding parameters for this basis are taken from the zinc-blende model of Ref. 15. This model considers only nearest-neighbor resonance integrals or hopping matrix elements, whilst the bulk crystal field splitting between the A and B valence subbands in bulk semiconductors with hexagonal lattice structure (the ''A-B'' splitting) cannot be reproduced unless third-nearest-neighbor interactions are taken into account.[22] To reproduce the A-B splitting within the sp^3s^* basis, we therefore add an additional -40 meV to the on-site energy of both Cd and Se p_z orbitals. When spin-orbit coupling is also included, this additional term gives a splitting of ~ 26 meV at the Γ point for the bulk crystal, in agreement with experiments.[23] The atomic basis parameters are transformed into a local sp^3s^* basis as follows. Each atom has one ''bonding'' hybridized orbital pointing at each of its immediate neighbors. There are two different local environments for the two types of atoms in the wurtzite unit cell,[24] and as a result, there are two types of hybridizations for each.[25] The wurtzite valence bands that result from transplanting the zinc-blende parameters are in good agreement with Ref. 26, while the conduction bands are slightly too flat [see Fig. 2(a) and Ref. 25]. Surface reconstruction of the clusters is not explicitly considered in this work. Such surface effects can be significant, and can be modeled using the total-energy minimization method of Ref. 26. Such considerations are reported elsewhere.[21]

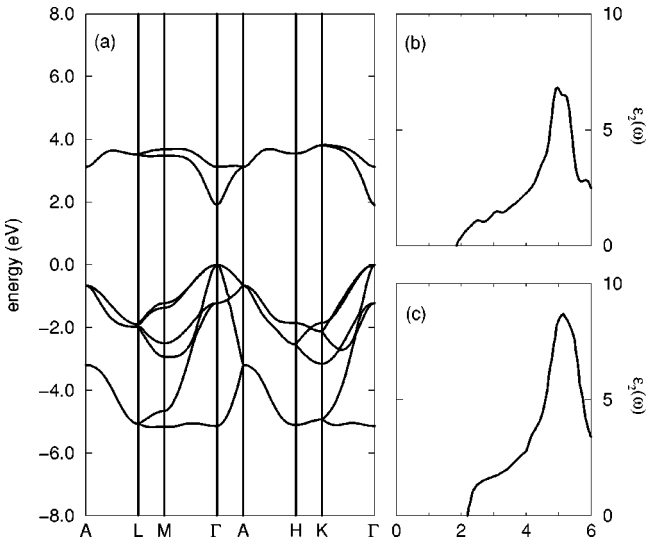

FIG. 2. (a) Wurtzite bulk band structure obtained using the parameters described in this work. (b) and (c): wurtzite CdSe bulk absorption spectrum for light polarized in the z direction (i.e., along the C_{3v} axis). (b) Predictions from the tight-binding model of this work; (c) LDA calculation of Ref. 40.

B. Restricted basis set diagonalization

The electron-hole two-particle Hamiltonian for tight-binding semiconductor nanocrystals is described in Ref. 18. Here we only briefly review its qualitative features. The two-particle basis is $|eh\rangle|j_sm_s\rangle$, where $|e\rangle$ and $|h\rangle$ are, respectively, eigenstates in the conduction and valence bands of the single-particle Hamiltonian without electron spin, and j_s and m_s are the total spin quantum numbers. The zeroth-order, diagonal terms of the two-particle Hamiltonian is therefore $\epsilon_e-\epsilon_h$, the difference between the conduction and valence single-particle energies. At this level of description, the singlet ($j_s=0$) and triplet ($j_s=1$) states are degenerate.

Coulomb, exchange, and spin-orbit couplings are then added as a perturbation,

$$\Delta\mathcal{H}=\begin{pmatrix} \mathcal{H}_{\rm coul}+\mathcal{H}_{\rm so}^{11;11} & \mathcal{H}_{\rm so}^{11;10} & \mathcal{H}_{\rm so}^{11;1\bar{1}} & \mathcal{H}_{\rm so}^{11;00} \\ \mathcal{H}_{\rm so}^{10;11} & \mathcal{H}_{\rm coul}+\mathcal{H}_{\rm so}^{10;10} & \mathcal{H}_{\rm so}^{10;1\bar{1}} & \mathcal{H}_{\rm so}^{10;00} \\ \mathcal{H}_{\rm so}^{1\bar{1};11} & \mathcal{H}_{\rm so}^{1\bar{1};10} & \mathcal{H}_{\rm coul}+\mathcal{H}_{\rm so}^{1\bar{1};1\bar{1}} & \mathcal{H}_{\rm so}^{1\bar{1};00} \\ \mathcal{H}_{\rm so}^{00;11} & \mathcal{H}_{\rm so}^{00;10} & \mathcal{H}_{\rm so}^{00;1\bar{1}} & \mathcal{H}_{\rm coul}+\mathcal{H}_{\rm ex}+\mathcal{H}_{\rm so}^{00;00} \end{pmatrix}, \tag{2}$$

where the Coulomb, exchange, and spin-orbit matrix elements are themselves matrices in the $|eh\rangle$ space, and the superscripts in $\mathcal{H}_{\rm so}^{j_s'm_s';j_sm_s}$ are the total spin labels. These matrix elements are computed by expanding the zeroth-order wave functions in the local, hybridized tight-binding basis set. The Coulomb and exchange matrix elements are computed using Slater orbital wave functions and phenomenological screening functions (see Appendix A and Ref. 18). The interactions couple the electron-hole states; in particular, the exchange interaction lifts the degeneracy between the spin-multiplets [Eq. (2)]. The spin-orbit coupling assumes only on-site terms.[28] The two types of atoms are assigned phenomenological spin-orbit coupling constants of $\lambda_{\rm Cd}=0.151$ eV and $\lambda_{\rm Se}=0.32$ eV, respectively.[29] With our tight-binding parameters, these coupling constants split the highest occupied bulk valence states by 0.42 eV at the Γ point, in good agreement with experiments.[23] In general, spin-orbit coupling mixes the singlet and triplet manifolds. As a results, the eigenstates of the two-particle Hamiltonian all contain finite singlet character.[17,18]

Since only the band-edge exciton states are of interest, we diagonalize the two-particle Hamiltonian with respect to a restricted set of band-edge valence and conduction wave functions and increase the basis set size until convergence is achieved. Implicit in this treatment is a first-order ''configuration interaction'' approximation, such that multiple excitations from the ground state are not explicitly considered. Multiple excitations lead to important screening effects which will be treated phenomenologically.

Due to the semiempirical nature of the tight-binding representation used here, the finer details of the numerical results reported here are somewhat dependent on the parameters chosen. Nevertheless, the electron-hole attraction for a single electron-hole state computed using our treatment of the Coulomb interactions is in agreement with standard perturbative results,[14,30] and the basic features of the results are seen to be a function of the level of microscopic description, rather than of any gross parametrization.

There are two major differences between our formulation and earlier two-particle tight-binding calculations:[17] (a) the short ranged exchange interactions are unscreened, as is required by the diagrammatic expansion of the irreducible two-particle vertex[18,31–33] (see Appendix A for a detailed discussion); (b) nearest-neighbor exchange integrals are included. We have previously implemented the current two-particle formulation for silicon nanocrystals, where it accounts well for the two-state (triplet-singlet) explanation of luminescence experiments, yielding good agreement with the Stokes shifts and radiative lifetimes of the luminescing states.[18] In the tight-binding model for CdSe, the conduction (electron) and valence (hole) states are concentrated on different species, i.e., Cd and Se, respectively, with relatively small on-site overlaps. As a result, we find that the nearest-neighbor exchange integrals and the long-ranged Coulomb term in the exchange matrix elements can be significant.

C. Dipole matrix elements

The ground-state absorption spectrum is given by[28]

$$\epsilon_2(\omega)=\frac{8\pi^2e^2\hbar^2}{3m_e^2\Omega}\sum_f E_{fG}^{-2}M_{fG}^2\delta(\omega-E_{fG}), \tag{3}$$

where f and G label the final and initial many-electron states, E_{fG} is the transition energy, m_e is the electron mass, Ω is the volume of the system, $M_{fG}^2=|\langle f|\hat{\mathbf{p}}|G\rangle|^2$ is the squared transition dipole matrix element between states f and G, and $\hat{\mathbf{p}}$ is the momentum operator. In the dipole approximation, spin flips are not allowed in optical transitions, and only the singlet component can absorb light. When exciton and spin-orbit effects are included, $(i\hbar/m_e)M_{fG}$ is given by

$$\langle\Psi_k^{(2)}|[\hat{\mathbf{r}},\hat{H}]|G\rangle=-E_k^{(2)}\sum_{ehj_sm_s}\psi_{eh;j_sm_s}^{k*}\langle e|\hat{\mathbf{r}}|h\rangle\delta_{j_s0}\delta_{m_s0}, \tag{4}$$

$$\langle e|\hat{\mathbf{r}}|h\rangle=\sum_{ii'\gamma\gamma'}c_{e;i\gamma'}^{*}c_{h;i\gamma}[\mathbf{r}_i\delta_{ii'}\delta_{\gamma\gamma'}+\langle i'\gamma'|\delta\hat{\mathbf{r}}_i|i\gamma\rangle], \tag{5}$$

where $|\Psi_k^{(2)}\rangle=\Sigma_{ehj_sm_s}\psi_{ehj_sm_s}^k|eh\rangle|j_sm_s\rangle$, (i,γ) is the atom/orbital label of the localized basis set, $E_k^{(2)}$ is the two-particle eigenenergy for state $|\Psi_k^{(2)}\rangle$, and we have used the convention $E_G=0$.

The first term in Eq. (5) is computed for nanocrystals by directly applying the $\hat{\mathbf{r}}_i$ operator, which gives the position of the tight-binding sites.[18] In the bulk phase, it is efficiently computed by applying the relation[34,35]

$$[\hat{\mathbf{r}},\hat{H}]\rightarrow-i\nabla_{\mathbf{k}}\mathcal{H}_{\mathbf{k}} \tag{6}$$

to atoms in one unit cell, where $\mathcal{H}_{\mathbf{k}}=\mathcal{U}_{\mathbf{k}}^{+}\mathcal{H}\mathcal{U}_{\mathbf{k}}$ is (in our case) the bulk CdSe unit-cell Hamiltonian matrix for the four atoms at positions $\mathbf{t}_j$, $j=1,2,3,4$, multiplied by the transformation matrices of Bloch phase factors whose diagonal terms are $e^{-i\mathbf{k}\cdot t_j}$.[36]

The second term in Eq. (5) is undefined in semiempirical tight-binding models, and can be adjusted to fit to experimental and/or *ab initio* results.[37–39] For $i\neq i'$, we must have $\langle i'\gamma'|\delta\hat{\mathbf{r}}_i|i\gamma\rangle=\langle i'\gamma'|\delta\hat{\mathbf{r}}_{i'}|i\gamma\rangle$, due to the assumed orthonor-

mality of the orbital basis functions. As in the case of exchange integrals, we only consider $i=i'$ and nearest-neighbor pairs (i,i'). In this work, the only nonzero transition dipole matrix elements are

$$\langle is^*|\delta\hat{\mathbf{r}}_i|ip_z\rangle = 0.4\mathbf{e}_z \text{ a.u.}, \quad i \text{ on Cd};$$
$$\langle i\gamma|\delta\hat{\mathbf{r}}|i'\gamma'\rangle = 1.8\mathbf{e}_z \text{ a.u.}, \quad i,i' \text{ nearest neighbors}, \quad \gamma,\gamma' \text{ bonding orbitals}, \tag{7}$$

where $\mathbf{e}_z$ is the unit vector in the z direction. The resulting z-polarized bulk absorption spectrum is shown in Fig. 2(b). Our choice of nearest-neighbor parameters gives a first-shoulder–to–first-peak ratio in reasonable agreement with local-density approximation (LDA) results.[40] The overall agreement in the energy range $E<6$ eV is reasonable, although our spectrum is smaller in magnitude. Similar agreement is found for the x- and y-polarized spectra.

D. Effective mass approximation

Theoretical understanding of exciton fine structure in direct gap material nanocrystals is mostly based on the multiband EMA theory, with the additional restriction of just one contributing electron state and three degenerate p-like valence states.[1] For a spherical EMA crystallite, with only spin-orbit coupling incorporated in the zeroth-level description, the lowest excitonic level formed from the band-edge electron and hole eigenstates is eightfold degenerate. The crystal-field splitting (Δ_{int}), shape asymmetry (Δ_{sh}), and the effect of the exchange interactions (η_o) are treated as perturbations. The Hamiltonian matrix is a function of Δ and η_o, where $\Delta=\Delta_{\text{sh}}+\Delta_{\text{int}}$. The exchange interaction is assumed to be short ranged. Hence $\eta_o \propto a^{-3}$, where a is the nanocrystal radius, and the resulting exchange contribution can be substantially enhanced over the bulk exchange splitting of 0.13 meV.[41] The crystal-field splitting $\Delta_{\text{int}} \approx 26$ meV and gives rise to the ''A-B'' splitting in bulk CdSe, while Δ_{sh} is strongly size dependent and is the dominant perturbation for small crystallites. Δ_{sh} is of the same sign as Δ_{int} in highly oblate CdSe crystallites, while the two factors tend to cancel in prolate tops.[1]

These interactions split the eightfold degenerate band edge states into five distinct levels, whose energies and oscillator strengths are strongly dependent on the nanocrystal shape. In Ref. 1 the levels are labeled according to their total angular momentum projection along the c axis of the nanocrystal. They can also be classified according to their spin origin as singlet and triplet states. (The dipole forbidden, purely triplet states are the ± 2 and 0^L states in the notation of Ref. 1.) Spherical and oblate CdSe nanocrystals exhibit a $\underline{2}:2:\underline{1}:2:1$ splitting pattern and no strong variation in oscillator strengths, where ''1'' and ''2'' indicate the degeneracies, and the underscores denote triplet states with infinite lifetimes.[1] For highly prolate CdSe crystallites, the EMA theory predicts a $\underline{1}:2:1:\underline{2}:2$ splitting pattern for the sizes of interest.[1] It also predicts that the oscillator strengths of the fifth level exceed that of the second level by a factor of 20 in small nanocrystals (the third level has intermediate oscillator strength), and suggests that this might explain the ~ 100 meV nonresonant Stokes shift observed in luminescence experiments.[1]

TABLE II. Energies, spatial extent, and polarization-averaged transition dipole matrix elements of the first few valence states of a sample nanocrystal. R_{xy}^2 and R_z^2 measure the mean squared radius of the valence wave functions in the respective directions about the wave function's electronic center of mass. M_{1h} connects valence state $|h\rangle$ with the lowest conduction state. The asterisks indicate valence states that dominate the lowest exciton (triplet) state in the presence of the Coulomb interaction.

Crystal/state	Energy (eV)	R_{xy}^2(Å^2)	R_z^2(Å^2)	$\lvert M_{1h}\rvert^2$(Å^2)
823 $\lvert h_1\rangle$	−0.2570	54.9	26.7	1×10^{-17}
823 $\lvert h_2\rangle$*	−0.3153	31.2	21.9	4.0
823 $\lvert h_3\rangle$*	−0.3153	31.2	21.9	4.0
823 $\lvert h_4\rangle$	−0.3269	36.4	56.7	5×10^{-3}
823 $\lvert h_5\rangle$	−0.3269	36.4	56.7	5×10^{-3}
823 $\lvert h_6\rangle$	−0.3560	20.8	49.4	4.4

These features provide useful guidelines for qualitatively intepreting the tight-binding exciton spectra. The tight-binding description introduces a more complete basis than the EMA, does not invoke the restrictive envelope function approximation, and explicitly takes the atomic geometry of the surface into account. As a result, the composite angular momentum labels cited in Ref. 1 are no longer good quantum numbers and several of the other characteristics above change significantly, as will be shown in the next section.

III. TIGHT-BINDING RESULTS

The single-particle states $|e\rangle$ and $|h\rangle$ are computed using an eigenvalue-selective Lanczos algorithm.[42,43] All the crystallites studied here have singly degenerate highest occupied valence states and doubly degenerate next-highest valence states, regardless of their moment of inertia ratios. This degeneracy pattern is consistent both with crystal-field splitting and the C_{3v} point group symmetry of the nanocrystals.[19] The highest singly degenerate HOMO state (A symmetry) is made up predominantly of p_x and p_y character, while the next-highest, doubly degenerate valence states (E symmetry) also contain some p_z character. For significantly more prolate nanocrystals, the order of these A and E states can be reversed.[25] In general the HOMO does not contribute to the band-edge fine structure once spin-orbit coupling is included, i.e., it is lowered in energy more than the next-highest valence states.

The Coulomb interaction and spin-orbit coupling cause a reordering of single-particle valence states. Consider the electronic levels of the 823-atom nanocrystal from series D (Table I). When only spin-orbit coupling is considered, the second through sixth single-particle valence states $h=2\ldots6$ all contribute to the lowest exciton state. Incorporation of the electron-hole attraction changes this picture. Now the states $h=2$ and 3 exhibit considerable overlaps with the lowest conduction state ($e=1$), while the others do not. The polarization-averaged transition dipole matrix elements $|M_{1h}|^2$ are a good measure of such overlaps. These are listed in Table II for the first six valence states of the 823-

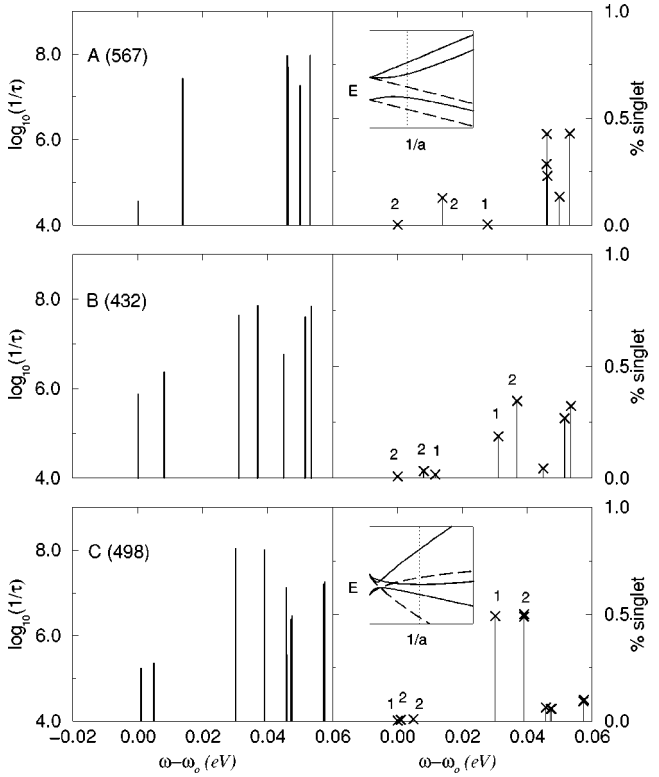

FIG. 3. Exciton fine structure for one crystallite each in series A (moments-of-inertia ratio 1.05:1:1, corresponding to $\mu_{\rm mir}=0.025$), B (1.2:1:1, $\mu_{\rm mir}=0.095$), and C (1.44:1:1, $\mu_{\rm mir}=0.20$). The frequencies are measured from ω_o, the lowest-lying exciton state. Left panel: relative oscillator strengths, defined in terms of the radiative recombination lifetimes τ (see text). Right panel: fractional singlet character. From top to bottom: series A, 567 atoms (14.0 Å radius), $\omega_o=2.4086$ eV; series B, 432 atoms (12.2 Å radius), $\omega_o=2.4995$ eV; series C, 498 atoms (12.8 Å radius), $\omega_o=2.4727$ eV. The numbers ''1'' and ''2'' denote the degeneracies. Insets: illustrations of the fine structure predicted by EMA, from Ref. 1. These show the energy splittings predicted for the first five levels as a function of inverse size $1/a$. The solid and dashed lines represent states of finite and infinite lifetimes, respectively. For their degeneracies; see text. The dotted line indicates in each case the crystallite size with which the tight-binding energy splittings are to be compared.

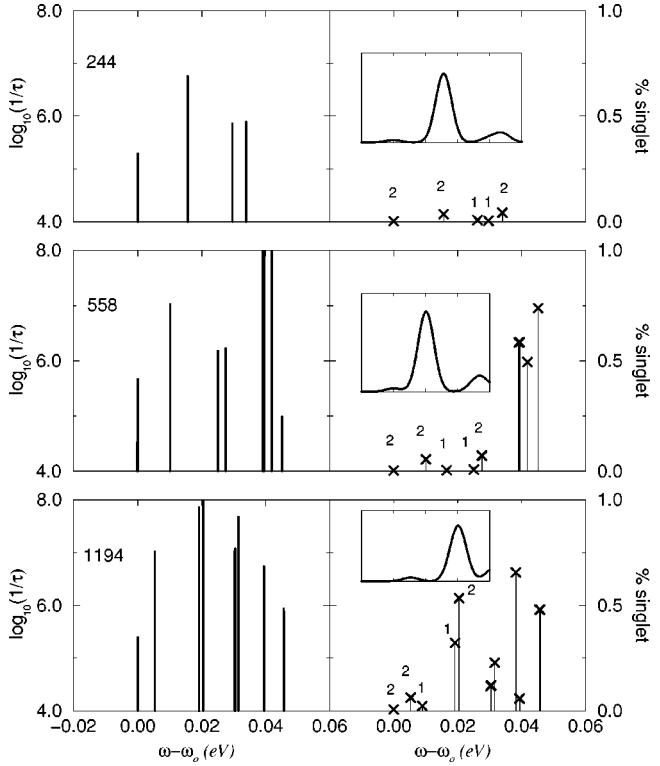

FIG. 4. Exciton fine structure for series D, whose moments of inertia ratio are within 3% of experimental aspect ratios [Eq. (1) and Ref. 1]. From top to bottom: 244 atoms (10.4 Å radius), $\omega_o=2.7405$ eV; 558 atoms (14.0 Å radius), $\omega_o=2.4086$ eV; 1194 atoms (18.3 Å radius), $\omega_o=2.2533$ eV. For symbols, refer to the figure caption of Fig. 3. Insets: $\epsilon(\omega)$ for the crystallites, broadened by a Gaussian with half-width 0.0025 eV.

atom nanocrystal. Larger overlaps mean larger electron-hole attraction, and consequently the two-particle states involving $h=2$ and 3 supplant those made up of $h=4$, 5, and 6 (see Table II). This implies that the Coulomb interaction can play a significant role in the fine structure of nanocrystals.

The restricted basis set method of Sec. II B is applied to a subset of single-particle states close to the band edges. ω_o, the energy of the lowest exciton state, is estimated to be accurate to within 5 meV for a basis set consisting of 24 valence and 18 conduction single-particle states. [Incorporation of spin makes the total basis size then $4\times24\times18$ (Ref. 18).] The energy *differences* between the exciton levels converge more rapidly. The level 1–level 2 splitting is converged to within 0.1 meV for the smaller crystallites and ~0.3 meV for the larger ones, while the relative errors in levels 3, 4, and 5 are estimated to be ~1–2 meV. For states beyond 0.1 eV from the band edge, the error in eigenenergies can be up to 30 meV. The band gaps of the nanocrystals, after the incorporation of exciton effects, are within 0.1–0.2 eV of the experimental first absorption peaks (see the figure caption of Fig. 4 and Ref. 44), and are also in good agreement with the perturbative estimates of Ref. 45. A previous tight-binding study that used a Coulomb interaction similar to the one used here overestimates the band gap by ~0.5 eV.[14] The discrepancy between that work and the present study can be attributed to the inclusion of spin-orbit effects and the difference in crystal lattice structure (wurtzite here versus zinc blende in Ref. 14).

In the absence of spin-orbit coupling, the Hamiltonian matrix in Eq. (2) is block diagonal, and the two-particle states are unambiguously singlets and triplets. Spin-orbit coupling mixes the pure singlets and triplets. Nevertheless, the finite exchange interactions still give rise to low-lying exciton states that are predominantly triplets and ''dark,'' in addition to higher-lying states that exbihit considerable oscillator strengths and that have systematically greater singlet character. In the absence of $\mathcal{H}_{\rm ex}$, all band-edge states luminesce with lifetimes 10^{-8} sec. This would be in marked disagreement with experiments, which show lifetimes greater than 10^{-6} sec.[1] Figure 3 shows the exciton fine structure and the fractional singlet character, $|\langle f|00\rangle|^2$, of a few exciton states $|f\rangle$ for a typical crystallite from each of the series A–C. In all cases, the first exciton level is at least 99% triplet. Also shown are the relative oscillator strengths, $\log_{10}(1/\tau)$, defined in terms of the radiative lifetimes $\tau=\tau_{fG}$, where[46]

$$1/\tau_{fG}=\frac{4ne^2E_{fG}^3|\mathbf{r}_{fG}|^2}{3\hbar^3c^3}. \quad (8)$$

Here $n=2.6$ is the bulk refractive index,[23] c is the speed of light, and e is the electronic charge.

We first consider the effects of crystallite ellipticity. The crystallites represented in Fig. 3 have roughly the same size, so the differences in fine structure are attributed to their different ellipticities. The qualitative EMA predictions for similar ellipticities are shown in each instance in the inset. Clusters in series *A* have almost spherical moments of inertia ratios. The major difference between their fine structure and EMA results for spherical crystallites in series *A* is that the first (and third) level, which is predominantly triplet, has a radiative lifetime of 10^{-4} to 10^{-5} sec, and not the infinite lifetime predicted by EMA, while the second level exhibits considerable singlet character and lifetimes that are two to three orders of magnitude smaller. The large disparity between the radiative lifetimes of the first two levels, coupled with their $\sim$10 meV energy splitting, is consistent with the fast and slow radiative decays observed in resonant luminescence experiments.[1] The finite lifetime arises from the atomic nature of the crystallite interior within the tight-binding description, in particular, the mixing of all three atomic *p* orbitals in the hole component. This is demonstrated explicitly in Appendix B, and is an important consequence of using a molecular level description of the crystallite. In contrast, because of the restriction to a single electron-hole pair state contributing to the exciton level, the EMA calculations of Ref. 1 predict that the lowest exciton level is purely triplet and therefore has infinite lifetime. As a result, other mechanisms are required to explain the finite time scale of the slow component.[1,10] The degeneracies of the first few states also correspond to the EMA predictions (see Sec. II D). The splittings between the first few excitonic states differ quantitatively in Fig. 3, partly because of the differences in ellipticity used here and in Ref. 1.

For series *B*, the degeneracies of the first two levels are the same here as in EMA, and both theories predict that the spacings between levels generally decrease with increasing size. However, in contrast to the EMA predictions, here the first two levels exhibit similar radiative lifetimes, so that there are no clear cut ''dark'' or ''bright'' states at the band edge. This nanocrystal series appears to be in the crossover regime between spherical and prolate in terms of its crystal shape (ellipticity $\mu_{\rm mir}=0.095$), and the lifetimes of the first two levels thus exhibit behavior intermediate between those of series *A* and *C*.

The crystallites in series *C* are prolate in shape, with $\mu_{\rm mir}=0.20$. Here the degeneracies of the first two levels exhibit a crossover as a function of size, with the lowest dark state switching from singly degenerate to doubly degenerate as the size increases. This is similar to the EMA predictions shown in the inset of panel *C* in Fig. 3. (The degeneracy crossover for large nanocrystals occurs at somewhat larger sizes in our calculations than in the EMA computations from Ref. 1, which is attributable to the slightly larger ellipticity value of $\mu=0.28$ used in Ref. 1.) We find that the lowest exciton states for the two smallest crystallites are at least 99% triplet, and exhibit extremely long ($\sim10^{-2}$–10^{-3} sec) radiative lifetimes, while the next-lowest states have considerably more singlet character, and have lifetimes of order 10^{-6} seconds. The oscillator strength of the first ''bright'' level is much smaller than that of states higher in the manifold. The small splittings, the change in the degeneracy of the first level as the size increases, and the distribution of oscillator strengths are in qualitative agreement with the EMA predictions at large sizes. There are important differences, however, the most obvious of which is the finding of long but nevertheless finite radiative lifetimes for the nominally triplet states, as was already noted for the spherical crystallites above. In addition, (a) the ordering of the higher levels are quite different; (b) the ''second'' dark level predicted by EMA is absent in the largest nanocrystal; and (c) the spacings amongst the first eight exciton states in our work are substantially smaller than those predicted by the EMA, particularly for the smallest nanocrystal, indicating a breakdown of the continuum theory at sizes below $\sim$12 Å radius.

In general, the spacings between the tight-binding exciton levels decrease with increasing crystallite size, again in agreement with EMA. Due to space limitations, the size dependences of the exciton fine structure for series *A*–*C* are not explicitly shown.

In Fig. 4, we show exciton fine structure and fractional singlet character for several nanocrystals in series *D* (244 atoms, 10.4 Å radius; 558 atoms, 14.0 Å radius; and 1194 atoms, 18.3 Å radius). For this series, the moments of inertia ratios are within 3% of the experimental TEM distribution,[1] and the larger crystallites are progressively more prolate (Table I).

The exciton fine structures are generally similar to that shown for series *A* in Fig. 3, with two quantitative differences, both of which can be attributed to the more prolate shape of the larger crystallites in this series. (a) The exchange splitting, and spacing between states are in general smaller than those for series *A* in Fig. 3. (b) The difference in radiative lifetimes of the bright and dark band-edge states are smaller. Instead of the 2–3 orders of magnitude difference found in the top panel of Fig. 3, the radiative lifetimes of the lowest-lying states are generally in the range 2×10^{-6} to 10^{-5} sec (5 of the 24 clusters in this series have band-edge lifetimes between 10^{-4} and 10^{-5} sec), while the first bright states have lifetimes smaller than 2×10^{-7} sec. These values are in good agreement with the experimental values of Ref. 1, where microsecond lifetimes were measured for the low-lying dark states. The lifetimes of the two levels thus differ by factors of 10–1000, with a median factor of about 30. Both features (a) and (b) can be attributed to the more prolate shape of the larger crystallites.

There are three interesting exceptions in the individual nanocrystals included in this series (Table I). (i) The 387-atom nanocrystal shown in Fig. 1 has a pronounced triangular shape when viewed along the *z* axis, whereas all other crystallites in this series have roughly hexagonal cross sections. The band-edge states of this particular crystallite all exhibit lifetimes smaller than 10^{-6} sec, and there are no clear-cut dark states. (ii) The 549-atom crystal has anomalous oscillator strength distributions, such that the ''bright'' band-edge states have lifetimes only three times smaller than the ''dark'' states below them, despite an order of magnitude

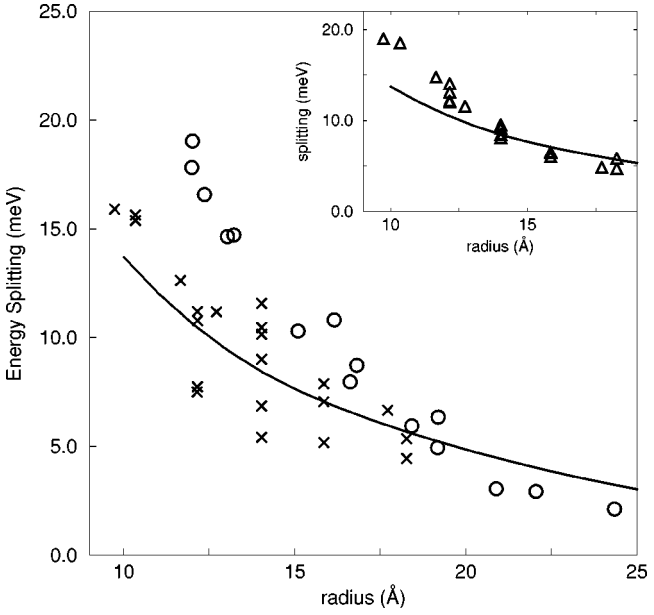

FIG. 5. Comparison of exchange interaction-induced Stokes shift for series *D* (crosses) with experimental resonant Stokes shifts (Ref. 1) (circles) and EMA predictions (solid line).[1] In the inset, the triangles are perturbative estimates [see text and (Ref. 47)].

difference in singlet character between them. (iii) The aspect ratio of the largest nanocrystal (1236 atoms), for which results are shown in Fig. 4, approaches that of series *B*, in accordance with the general observation that larger crystallites are more prolate in shape.[2] As a result, its fine structure begins to resemble those shown in the middle panel of Fig. 3, and the radiative lifetimes for the first two levels are 10^{-6} and 5×10^{-6} sec, i.e., are separated by only a factor of 5.

Figure 5 compares the splitting between the lowest dark and bright states for series *D* nanocrystals with the EMA predictions for the corresponding ideal ellipsoids, and also with the resonant Stokes shifts derived from the experimental fluorescence line narrowing results.[1] In accordance with the EMA language used there, we shall loosely refer to this as the exchange splitting. The average exchange splittings obtained here are in agreement with the EMA estimates over a wide range of effective crystal radii. The splittings are not monotonic, but exhibit considerable ''noise'' for each size. This is due partly to the 3% deviation in moments of inertia ratios from the experimentally observed distribution (Table I). However, it is also due in part to the atomic nature of the crystallites. Thus clusters with similar moments of inertia ratios and/or length-to-width ratios can adopt significantly different physical shapes. In addition, we note that the noise in the splittings is also affected by the mixing in of states beyond the band-edge electron-hole states. The exchange splittings estimated perturbatively,[47] shown in the inset of Fig. 5, exhibit considerably less noise. The mean value of our splittings are in reasonable agreement with experiments for the largest crystallites considered. The theoretical and experimental values appear to converge at about radius 20 Å. For small cluster sizes, both the tight-binding and EMA results are smaller than the experimental resonant Stokes shifts.

Several factors may contribute to the differences between experimental and theoretical estimates for resonant Stokes shifts at small nanocrystal sizes. The first, and apparently most important, is the fact that surface structure and relaxation effects have been totally neglected in both the EMA and in these truncated cluster calculations. Total-energy minimization calculations, to be described in detail elsewhere,[21] show that the exchange splitting is significantly raised for smaller crystallites and achieve good agreement with the experimental resonant Stokes shifts, decreasing also the shape dependent ''noise'' seen in Fig. 5.

A second effect is the uncertainty in the shape measurements of the nanocrystals. In the EMA and in the experiments,[1] length-to-width estimates are applied to extract these, and the uncertainty in the experimental aspect ratios is unknown. The aspect ratios of the crystallites studied here in series *D* are estimated from the moments-of-inertia ratios. As discussed in Sec. II A and illustrated in Table I, this typically predicts a slightly different shape than the corresponding length-to-width based estimate (μ_{physical}) of the crystallite in question would indicate. As mentioned earlier however, the length-to-width based procedure would give misleading shape assignments for the size range considered here.

In addition to the resonant Stokes shifts, Ref. 1 also analyzed the size-dependent nonresonant Stokes shifts in terms of the exciton fine structure.[1] In the nonresonant case, excitation is made above the band-edge absorption. The relevant states in EMA theory are the fourth and fifth exciton levels, both of which have considerably larger oscillator strengths than the second level, which is the first optically bright level and is responsible for the resonant Stokes shifts. EMA predicted nonresonant Stokes shifts that are smaller than experimental values.[1,10] In the tight-binding model, we can make a similar estimate by considering the difference between ω_o and the eigenenergy of the first two-particle state higher up in the exciton manifold having oscillator strengths 10–20 times larger than the band-edge bright state. We find that these energy shifts also underestimate the experimental nonresonant Stokes shift by at least a factor of 2, similar to EMA. In this case, when surface relaxation is then included, the oscillator strengths of the band-edge bright states increase, and there are no higher-lying states with order-of-magnitude difference in oscillator strengths.[21] Therefore we conclude that unlike the resonant Stokes shift, the nonresonant Stokes shift does not appear to be attributable to fine-structure effects alone.

IV. SUMMARY AND DISCUSSIONS

We have made a study of the excitonic fine structure in CdSe nanoclusters that incorporates electron-hole and spin-orbit interactions within an underlying tight-binding model for the electronic structure. This work goes beyond the EMA treatment in that it incorporates details on atomic length scales, and also includes the effect of many more electronic states than those derived merely from the eight valence-band-edge states. It therefore constitutes a more complete treatment against which the EMA results can be compared.

The major differences between our findings and EMA predictions can be summarized as follows: (a) The existence of a ''dark,'' predominantly triplet band-edge excitonic state with finite rather than infinite lifetime is demonstrated in all four series of nanocrystals studied here. The finite lifetime

arises from the inclusion of atomic details in the tight-binding wave functions (see Appendix B). The lifetimes of these ''dark'' states are in order-of-magnitude agreement with experiments, even before introducing the additional effects of phonons. (b) For series D, i.e., crystallites with ellipticities derived from moments of inertia ratios that correspond to experimental ellipticities (derived from aspect ratios), the band-edge dark states have lifetimes predominantly in the 10^{-5}–10^{-6} s range, in order-of-magnitude agreement with experiments. This is significant, although a quantative comparison with experiments requires a distribution of sizes and shapes, as well as a consideration of the effects of coupling to phonons. (c) The importance of the atomic nature of the wave functions seen here suggests that a more realistic treatment of the surface is warranted. For the smaller clusters, e.g., the 387-atom cluster, approximately half of the atoms lie on the surface. Thus a realistic modeling of the surface atoms and of the passivating ligands should be considered in these cases.[25] The effects of a molecular representation of the surface and of its reconstruction will be discussed elsewhere.[21] (d) The detailed structure of the higher EMA levels are not reproduced, because mixing between the eight lowest exciton states and the higher states is significant, especially for the smaller crystallites. This mixing is consistent with conclusions reached from recent measurements of dipole moments for colloidal CdSe nanocrystals[11] and two-photon fluorescence excitation spectra.[27]

Despite these differences, there are nevertheless some notable similarities between our tight-binding results and the EMA predictions. Thus, the degeneracies of the lowest three or four levels of the tight-binding crystallites are in agreement with EMA. Furthermore, the relative oscillator strengths for the ''bright'' states are in qualitative agreement for crystallite series with various ellipticities. The exchange-induced resonant Stokes shifts are also similar to EMA values,[1] albeit with considerable ''noise'' as a function of size resulting from the sensitivity of the size parameters to the discrete nature of the atomic level and shape details. Increased values for resonant Stokes shifts at smaller cluster sizes, resulting in better agreement with the experimental values, and a reduction of the noise in the exchange splittings can be obtained when surface relaxation effects are taken into account.[21]

ACKNOWLEDGMENTS

This work was supported by a grant from Sandia National Laboratories, Contract No. AR-9600, and by the Materials Design Initiative at Lawrence Berkeley National Laboratory, under ONR Contract No. N0001495F0099. Computations were performed at the San Diego Supercomputer Center under an allocation of computer time on the C90, and at the Pittsburgh Supercomputer Center under a grant on the supercluster. The authors thank Bruce Chou for his help in constructing the nanocrystal models and Huy Phung for performing some computations.

APPENDIX A: COULOMB AND EXCHANGE INTEGRALS, AND SCREENING

The tight-binding calculation is cast in the $(sp^3)^4s^*$ basis. The Coulomb and exchange integrals are $\langle sp_p^3 sp_q^3|(1/r)|sp_p^3 sp_q^3\rangle$ and $\langle sp_p^3 sp_q^3|(1/r)|sp_q^3 sp_p^3\rangle$, $p,q=a,b,c,d$. The on-site integrals are conveniently calculated in the $\{s,p_x,p_y,p_z,s^*\}$ basis using Slater orbital wave functions for cadmium and selenium atoms.[48] Integrals in the hybridized basis are then expressed in terms of the atomic integrals, discarding terms that involve more than two distinct atomic orbitals. Screening is applied phenomenologically using a dielectric function $\epsilon(r)$ taken from Ref. 49 to modify the $1/r$ bare interaction. For Coulomb interactions between electrons on the same atom, the effect of $\epsilon(r)$ is to rescale the bare Coulomb integrals by ≈ 0.51 for Se and 0.37 for Cd, respectively. For long-ranged Coulomb and exchange interactions, the Ohno formula[13,50] is applied. The short-ranged contribution to the exchange matrix element is unscreened,[31,33,51–53] and $\epsilon(r)$ is replaced by unity. For a discussion of this and for more computational details, see Ref. 18.

TABLE III. On-site Coulomb integrals in the sp^3s^* basis for Se (Cd), in units of eV. sp_a^3 and sp_b^3 refer to different sp^3 hybridized orbitals.

	sp_a^3	sp_b^3	s^*
sp_a^3	13.5254 (6.875)	10.1582 (5.147)	1.530 (0.462)
sp_b^3	10.1582 (5.147)	13.5254 (6.875)	1.530 (0.462)
s^*	1.530 (0.462)	1.530 (0.462)	1.230 (0.372)

This treatment of screening is approximate, as the demarcation of screened and unscreened contributions to exchange is quite complex.[51–53] Another issue for the exchange interaction is the contribution of the ''dipole''-like terms that arise from going beyond the ''pairwise overlap approximation'' made in Ref. 18, which discards terms involving two different orbital of the same atom. Such dipole interactions allow the exciton to propagate in bulk crystals.[54] Even when unscreened, these terms contribute less than 0.5 meV for the small crystallites studied here, and they decrease with crystallite size.

The resulting unscreened on-site Coulomb and exchange integrals in the sp^3s^* basis are listed in Tables III and IV, respectively, and the unscreened nearest-neighbor exchange integrals are listed in Table V. We note that the precise magnitudes of these integrals may depend on the orbital basis employed to evaluate them, here the Slater orbitals.

The perturbative exchange splitting shown in the inset of Fig. 5 can be increased by up to a factor of 2.5 if the long-ranged part is unscreened. Treated nonperturbatively, exchange splittings are less affected by the effect of this screening, but the resulting radiative lifetimes can differ by a factor of 5. Perturbative exchange splittings with unscreened long-ranged contributions have also been computed in Ref. 6.

TABLE IV. On-site exchange integrals in the sp^3s^* basis for Se (Cd), in units of eV.

	sp_a^3	sp_b^3	s^*
sp_a^3	13.5254 (6.875)	0.9243 (0.557)	0.000 (0.000)
sp_b^3	0.9243 (0.557)	13.5254 (6.875)	0.000 (0.000)
s^*	0.000 (0.000)	0.000 (0.000)	1.230 (0.372)

TABLE V. Nearest-neighbor exchange integrals for the sp^3 orbitals in units of eV.

	Cd: bonding	Cd: nonbonding
Se: bonding	1.427	0.347
Se: nonbonding	0.690	0.157

However, since the Coulomb interaction is not included to zeroth order in that calculation, the extent of singlet character of the lowest exciton (band-edge) states are unknown, rendering a direct comparison difficult.

APPENDIX B: ORIGINS OF THE FINITE SINGLET CHARACTER OF THE EXCITON GROUND STATE

When finite spin-orbit coupling and atomic details are included in the description of band-edge wave functions in nanocrystals, the lowest-lying band-edge exciton states lose their pure triplet status, and they acquire singlet character and finite lifetimes. We illustrate this here with a simple model. In our tight-binding model, the valence states typically have finite p_x/p_y and p_z contributions on each atom. In the nanocrystals studied here, the first dark and the first bright exciton levels are predominantly made up of a single s-like conduction state and two degenerate, p_x- and p_y-like valence states. This is especially true for small surface reconstructed crystallites,[21] where the p_z orbitals contribute less than 5% to the band-edge states, and p_z-dominated states are at least 0.1 eV away from band edge.

The valence p orbital populations differ from atom to atom, and depend on the location of the atom in the cluster. To mimic this effect in a transparent way, we consider a two-atom cluster, with artificially prescribed degenerate, orthonormal highest occupied valence states $|r\rangle$ and $|s\rangle$ given by

$$|r\rangle=\gamma|p_x;1\rangle+\delta|p_z;1\rangle+\gamma|p_x;2\rangle,$$
$$|s\rangle=\gamma|p_y;1\rangle+\gamma|p_y;2\rangle+\delta|p_z;2\rangle, \tag{B1}$$

where the second index labels atom 1 or 2. Some p_z contributions are thus allowed when $\delta\neq 0$. Converting the p_x and p_y orbitals to the spherical harmonic atomic basis $\{|m_l;\text{atom}\rangle\}$, $m_l=\pm 1,0$, we obtain

$$|a\rangle=\gamma|+1;1\rangle+(\delta/\sqrt{2})|p_z;1\rangle+\gamma|+1;2\rangle + i(\delta/\sqrt{2})|p_z;2\rangle,$$
$$|b\rangle=\gamma|-1;1\rangle+(\delta/\sqrt{2})|p_z;1\rangle+\gamma|-1;2\rangle - i(\delta/\sqrt{2})|p_z;2\rangle. \tag{B2}$$

Adding the spin-orbit coupling and exchange interaction perturbatively, the two-particle Hamiltonian becomes

$$\mathcal{H}=\begin{array}{c} \\ (a++)\\(a+-)\\(a-+)\\(a--)\\(b++)\\(b+-)\\(b-+)\\(b--)\end{array}\begin{array}{c}\begin{array}{cccccccc}(a++)&(a+-)&(a-+)&(a--)&(b++)&(b+-)&(b-+)&(b--)\end{array}\\ \begin{pmatrix} -\lambda_2 & 0 & \Delta & 0 & 0 & 0 & 0 & 0\\ 0 & -\lambda_2+\eta & -\eta & \Delta & 0 & 0 & 0 & 0\\ \Delta^* & -\eta & \lambda_2+\eta & 0 & 2\Delta & 0 & 0 & 0\\ 0 & \Delta^* & 0 & \lambda_2 & 0 & 2\Delta & 0 & 0\\ 0 & 0 & 2\Delta^* & 0 & \lambda_2 & 0 & \Delta & 0\\ 0 & 0 & 0 & 2\Delta^* & 0 & \lambda_2+\eta & -\eta & \Delta\\ 0 & 0 & 0 & 0 & \Delta^* & -\eta & -\lambda_2+\eta & 0\\ 0 & 0 & 0 & 0 & 0 & \Delta^* & 0 & -\lambda_2 \end{pmatrix}\end{array}, \tag{B3}$$

where $(a+-)$ (for example) denotes the two-particle state with spatial wave function $|a\rangle$, hole spin $|+\rangle$, and electron spin $|-\rangle$, $\lambda_2=\gamma^2\lambda/2$ is proportional to the spin-orbit coupling constant λ, η is the exchange integral, $\Delta=-(1-i)\lambda\gamma\delta/2$, and the band-gap energy ω_o and the Coulomb terms have been set equal to zero. The parameter Δ provides an indication of the extent of mixing between singlets and triplets. Note that the basis set in the above is different from that used in Eq. (14) of Ref. 1.

When $\delta=0$, we have purely p_x and p_y waves. The band-edge states $|a++\rangle$ and $|b--\rangle$ are pure triplets. In the limit that $\lambda\gg\eta$, the next-lowest states are $|a+-\rangle$ and $|b-+\rangle$, lying at an energy η above the band edge. When projected into the singlet-triplet representation, these states are found to have 50% singlet character.

Small admixtures of p_z contributions to $|a\rangle$ and $|b\rangle$ render Δ nonzero. To $O(\Delta^2)$, $|a++\rangle$ and $|b--\rangle$ mix with $|a-+\rangle$ and $|b+-\rangle$, respectively. The latter are again 50% singlets, therefore effectively introducing singlet character and oscillator strength into the lowest excitonic states. Using the sample parameters $\lambda=0.324$ eV, $\eta=0.001$ eV, and $\delta=0.1$ (i.e., 1% p_z character in each valence state), we find that the lowest exciton (band-edge) states acquire 0.3% singlet character.

The above illustration uses a rather restricted set of basis states. However, in the detailed calculations carried out in this paper, we have found that inclusion of states further away from the band-edge states does not change the qualitative picture arrived at in this simple example by using only a few two-particle states. Hence the conclusion arrived at in this appendix appears quite general.

*Present address: Sandia National Laboratories, MS 1421, Albuquerque, New Mexico 87185.
†Present address: Institut für Physikalische Chemie, Universität Bonn, Wegelerstr. 12, 53115 Bonn, FRG.

[1] Al. L. Efros, M. Rosen, M. Kuno, M. Nirmal, D. J. Norris, and M. Bawendi, Phys. Rev. B **54**, 4843 (1996).
[2] D. J. Norris, Al. L. Efros, M. Rosen, and M. G. Bawendi, Phys. Rev. B **53**, 16 347 (1996).
[3] M. Nirmal, D. J. Norris, M. Kuno, M. G. Bawendi, Al. L. Efros, and M. Rosen, Phys. Rev. Lett. **75**, 3728 (1995).
[4] A. I. Ekimov, F. Hache, M. C. Schanne-Klein, D. Ricard, C. Flytzanis, I. A. Kudryavtsev, T. C. Yazeva, A. V. Rodina, and Al. L. Efros, J. Opt. Soc. Am. B **10**, 100 (1993).
[5] M. Chamarro, C. Gourdon, P. Lavallard, O. Lublinskaya, and A. I. Ekimov, Phys. Rev. B **53**, 1336 (1996).
[6] A. Franceschetti and A. Zunger, Phys. Rev. Lett. **78**, 915 (1997).
[7] S. Nomura, Y. Segawa, and T. Kobayashi, Phys. Rev. B **49**, 13 571 (1994).
[8] U. Woggon, F. Gindele, O. Wind, and C. Klingshirn, Phys. Rev. B **54**, 1506 (1996).
[9] In a summary, see D. J. Norris and M. G. Bawendi, J. Chem. Phys. **103**, 5260 (1995).
[10] M. Kuno, J. K. Lee, B. O. Dabbousi, F. V. Mikulec, and M. G. Bawendi, J. Chem. Phys. **106**, 9869 (1997).
[11] S. A. Blanton, R. L. Leheny, M. A. Hines, and P. Guyot-Sionnest, Phys. Rev. Lett. **79**, 865 (1997).
[12] N. A. Hill and K. B. Whaley, J. Chem. Phys. **100**, 2831 (1994); **99**, 3707 (1993).
[13] N. A. Hill and K. B. Whaley, J. Electron. Mater. **25**, 269 (1996).
[14] N. A. Hill and K. B. Whaley, Chem. Phys. **210**, 117 (1996).
[15] P. E. Lippens and M. Lannoo, Phys. Rev. B **41**, 6079 (1990); **39**, 10 935 (1989).
[16] L. M. Ramaniah and S. V. Nair, Phys. Rev. B **47**, 7132 (1993); S. V. Nair, L. M. Ramaniah, and K. C. Rustagi, *ibid.* **45**, 5969 (1992).
[17] E. Martin, C. Delerue, G. Allan, and M. Lannoo, Phys. Rev. B **50**, 18 258 (1994).
[18] K. Leung and K. B. Whaley, Phys. Rev. B **56**, 7455 (1997).
[19] J.-J. Shiang, A. V. Kadavanich, R. K. Grubbs, and A. P. Alivastos, J. Phys. Chem. **99**, 17 417 (1995).
[20] M. G. Bawendi, A. R. Kortan, M. L. Steigerwald, and L. E. Brus, J. Chem. Phys. **91**, 7282 (1989).
[21] K. Leung and K. B. Whaley (unpublished).
[22] A. Niwa, T. Ohtoshi, and T. Kuroda, Jpn. J. Appl. Phys., Part 2 **35**, L599 (1996).
[23] I. Broser, R. Broser, and A. Hoffmann, in *Numerical Data and Functional Relationships in Science and Technology*, edited by O. Madelung, M. Schulz, and H. Weiss, Landolt-Börnstein, New Series, Group III, Vol. 17, Pt. b (Springer-Verlag, Berlin, 1982), p. 202.
[24] A. Kobayashi, O. F. Sankey, S. M. Volz, and J. D. Dow, Phys. Rev. B **28**, 935 (1983).
[25] S. Pokrant and K. B. Whaley (unpublished); S. Pokrant, Diploma thesis (Philipps University, Marburg, Germany, 1996).
[26] Y. R. Wang and C. B. Duke, Phys. Rev. B **37**, 6417 (1988).
[27] M. E. Schmidt, S. A. Blanton, M. A. Hines, and P. Guyot-Sionnest, J. Chem. Phys. **106,** 5254 (1997).
[28] F. Bassani and G. Pastori Parravicini, *Electronic States and Optical Transition in Solids* (Pergamon, Oxford, 1975).
[29] D. J. Chadi, Phys. Rev. B **16**, 790 (1977).
[30] L. E. Brus, J. Chem. Phys. **80**, 4403 (1984).
[31] T. Takagahara and K. Takeda, Phys. Rev. B **53**, R4205 (1996).
[32] Y. Abe, Y. Osaka, and A. Morita, J. Phys. Soc. Jpn. **17**, 1576 (1962).
[33] L. J. Sham and T. M. Rice, Phys. Rev. **144**, 708 (1966).
[34] E. I. Blount, in *Solid State Physics*, edited by F. Seitz and D. Turnbull (Academic Press, New York, 1962), Vol. 13, p. 306.
[35] L. C. Lew Yan Voon and L. R. Ram-Mohan, Phys. Rev. B **47**, 15 500 (1993), and references therein.
[36] W. A. Harrison, *Electronic Structures and the Properties of Solids* (Dover, New York, 1989).
[37] Z.-Z. Xu, Solid State Commun. **76**, 1143 (1990).
[38] V. I. Gavrilenko and F. Rebentrost, Surf. Sci. **331-333**, 1355 (1995).
[39] R. Del Sole and R. Girlanda, Phys. Rev. B **48**, 11 789 (1993); A. Selloni, P. Marsella, and R. Del Sole, *ibid.* **33**, 8885 (1986).
[40] Y.-N. Xu and W. Y. Ching, Phys. Rev. B **48**, 4335 (1993).
[41] V. P. Kochereshko, G. V. Mikhailov, and I. N. Ural'tsev, Fiz. Tverd. Tela **25**, 769 (1983) [Sov. Phys. Solid State **25**, 439 (1983)].
[42] J. K. Cullum and R. A. Willoughby, *Lanczos Algorithms for Large Symmetric Eigenvalue Computations* (Birkhäuser, Boston, 1985), Vols. 1 and 2.
[43] The computer programs LEVAL and LEVEC are available from the archive at netlib@ornl.gov. Degeneracies are determined by repeating the diagonalization runs with different random seed numbers until no new states emerge.
[44] C. B. Murray, M. Nirmal, D. J. Norris, and M. G. Bawendi, Z. Phys. D **26**, S231 (1993); C. B. Murray, D. J. Norris, and M. G. Bawendi, J. Am. Chem. Soc. **115**, 8706 (1993).
[45] L.-W. Wang and A. Zunger, Phys. Rev. B **53**, 9579 (1996).
[46] D. L. Dexter, in *Solid State Physics*, edited by F. Seitz and D. Turnbull (Academic Press, New York, 1958), Vol. 6, p. 355.
[47] To compute the perturbative exchange splittings, we first diagonalize the spin-orbit coupling in the valence states and select the lowest-energy single-particle state(s). The Coulomb interaction between the lowest-energy conduction state and these valence states is also included to zeroth order, which partially lifts the degeneracies at the edge of the valence band. The resulting lowest-lying electron-hole states are 25% singlets. The exchange interaction is then applied perturbatively to these zeroth-order states.
[48] J. C. Slater, Phys. Rev. **36**, 57 (1930).
[49] H. Haken, J. Phys. Chem. Solids **8**, 166 (1959).
[50] K. Ohno, Theor. Chim. Acta **2**, 219 (1964).
[51] V. A. Kiselev and A. G. Zhilich, Fiz. Tverd. Tela **14**, 1438 (1972) [Sov. Phys. Solid State **14**, 1233 (1974)].
[52] U. Rössler and H.-R. Trebin, Phys. Rev. B **23**, 1961 (1981).
[53] K. Ehara and K. Cho, J. Phys. Soc. Jpn. **51**, 3553 (1982).
[54] R. S. Knox, *Solid State Physics* (Academic Press, New York, 1963), Vol. 5, p. 1.